Bidirectional flow of the funny current (I_f) during the pacemaking cycle in murine sinoatrial node myocytes

Colin H. Peters[a] [ID], Pin W. Liu[b], Stefano Morotti[c] [ID], Stephanie C. Gantz[b,d], Eleonora Grandi[c] [ID], Bruce P. Bean[b], and Catherine Proenza[a,e,1] [ID]

[a]Department of Physiology and Biophysics, University of Colorado Anschutz Medical Campus, Aurora, CO 80045; [b]Department of Neurobiology, Harvard Medical School, Boston, MA 02115; [c]Department of Pharmacology, University of California, Davis, CA 95616; [d]Department of Molecular Physiology and Biophysics, Carver College of Medicine, University of Iowa, Iowa City, IA 52242; and [e]Department of Medicine, Division of Cardiology, University of Colorado Anschutz Medical Campus, Aurora, CO 80045

Sinoatrial node myocytes (SAMs) act as cardiac pacemaker cells by firing spontaneous action potentials (APs) that initiate each heartbeat. The funny current (I_f) is critical for the generation of these spontaneous APs; however, its precise role during the pacemaking cycle remains unresolved. Here, we used the AP-clamp technique to quantify I_f during the cardiac cycle in mouse SAMs. We found that I_f is persistently active throughout the sinoatrial AP, with surprisingly little voltage-dependent gating. As a consequence, it carries both inward and outward current around its reversal potential of −30 mV. Despite operating at only 2 to 5% of its maximal conductance, I_f carries a substantial fraction of both depolarizing and repolarizing net charge movement during the firing cycle. We also show that β-adrenergic receptor stimulation increases the percentage of net depolarizing charge moved by I_f, consistent with a contribution of I_f to the fight-or-flight increase in heart rate. These properties were confirmed by heterologously expressed HCN4 channels and by mathematical models of I_f. Modeling further suggested that the slow rates of activation and deactivation of the HCN4 isoform underlie the persistent activity of I_f during the sinoatrial AP. These results establish a new conceptual framework for the role of I_f in pacemaking, in which it operates at a very small fraction of maximal activation but nevertheless drives membrane potential oscillations in SAMs by providing substantial driving force in both inward and outward directions.

cardiac pacemaking | HCN channel | funny current | AP clamp | sinoatrial node

Each beat of the heart is initiated by spontaneous pacemaker activity that originates in the sinoatrial node (1). Sinoatrial node myocytes (SAMs) are specialized cardiomyocytes that function as pacemaker cells by generating spontaneous action potentials (APs). Sinoatrial APs differ considerably from the APs of working cardiomyocytes in the atrial and ventricular myocardium, reflecting the unique function and protein expression of SAMs. In addition to having a slower upstroke velocity and smaller amplitude, sinoatrial APs are characterized by a spontaneous depolarization during diastole that drives the membrane potential to threshold to trigger the next AP.

The funny current (I_f) is a hallmark of SAMs and is among the many ionic currents that are known to contribute to the generation of spontaneous APs in SAMs (2). I_f was first described in the late 1970s as a hyperpolarization-activated inward current that is increased by β-adrenergic receptor (β-AR) stimulation (3). I_f is produced by hyperpolarization-activated cyclic nucleotide–sensitive (HCN) channels, which were first cloned in the late 1990s (4). HCN4 is the primary HCN-channel isoform expressed in the sinoatrial node of all mammals (5, 6). I_f and HCN4 are known to be critical for pacemaking—pharmacological inhibition of I_f slows heart rate (7, 8), and mutations in HCN4 cause sinus arrhythmias in humans and animal models (9–11). However, there is still debate about the specific contribution of I_f to the sinoatrial AP in part because the steady-state voltage dependence and slow activation of the current seemingly preclude appreciable channel activity at

physiological potentials during the dynamic pacemaker cycle (12, 13).

I_f is generally described as an inward current, and its role in pacemaking is typically considered only in terms of the diastolic depolarization phase of the sinoatrial AP (9, 12, 14–16). However, its slow kinetics (6, 17), the presence of a voltage-independent component to HCN-channel current (18, 19), and its permeability to both Na^+ and K^+ with a net reversal potential around −30 mV suggest the possibility that I_f may remain active throughout the duration of the sinoatrial AP and that it may also conduct outward current. Indeed, in a review of eleven different computational models of I_f, Verkerk and Wilders show that all models produce some outward current during the upstroke and repolarization phases of the AP (20) despite the large variations between models due to differences in experimental conditions of the underlying data. Thus, I_f may also contribute to the repolarization phase of the sinoatrial AP, an important functional role that is typically not assayed in experiments.

Uncertainty about the role of I_f in shaping the sinoatrial AP is driven by the difficulty of directly measuring the current during the firing cycle. A fundamental limitation to studying the contribution of any individual current in SAMs is that manipulation of a single current—for example, by blockers or genetic knockout—alters the AP morphology and the activation of other currents, which, in turn, feedback to change the current of interest. This difficulty is further compounded by a large variability in sinoatrial AP waveforms and

Significance

The funny current (I_f) is critical for spontaneous activity in cardiac pacemaker cells; however, its precise role remains enigmatic because it activates mostly outside the physiological voltage range and its kinetics are slow relative to the cardiac cycle. I_f is typically considered as an inward current; however, we show that I_f is persistently active in pacemaker cells. Once opened, the small fraction of ion channels that conduct I_f do not reclose. Consequently, I_f flows both inward and outward and, paradoxically, conducts a large fraction of the net charge movement. These results establish a new conceptual framework for pacemaking in which voltage-dependent gating of I_f is minimal and I_f contributes to spontaneous pacemaker activity by providing driving force in both directions.

PHYSIOLOGY

I_f amplitudes, even within cells isolated from the same animal (21–23). This is to say nothing of the large effects that physiological changes such as age can have on the AP (24, 25). Finally, the measurement of I_f is limited by the lack of specific blockers that can be used to isolate I_f from other currents. Indeed, HCN-channel blockers such as ivabradine, ZD7288, zatebradine, cilobradine, and Cs^+ have been shown to also inhibit voltage-gated Ca^{2+}, K^+, and Na^+ channels (26–35).

To overcome these challenges and directly measure I_f during the sinoatrial AP, we developed a series of pharmacological blockers to minimize the off-target effects of ivabradine and then used the AP-clamp technique to isolate I_f as the ivabradine-sensitive current flowing in response to the AP in acutely isolated mouse SAMs. Our recordings revealed that I_f in SAMs is biphasic, flowing both inward and outward during the AP. The trajectory of I_f tracked that of the membrane potential remarkably closely, and current–voltage relationships indicated that there is little voltage-dependent gating (<10%) of I_f during the sinoatrial AP. These results were confirmed by heterologously expressed HCN4 channels and by mathematical models of I_f. Together the data suggest a new conceptual framework for the role of I_f in pacemaking, in which it operates at a very small fraction of maximal activation but nevertheless drives membrane potential oscillations in SAMs by providing substantial driving force in both inward and outward directions.

Results

Isolation of I_f as an Ivabradine-Sensitive Current in the Presence of Na^+, Ca^{2+}, and K^+ Channel Blockers.

In order to directly measure I_f during the AP in SAMs, we used the Food and Drug Administration (FDA)-approved drug ivabradine as a blocker because it appears to have somewhat higher specificity compared to other I_f inhibitors (32, 36, 37). To assess the degree of the block, acutely isolated SAMs from mice were voltage-clamped in the whole-cell configuration at 35 °C, and I_f was assayed in response to hyperpolarizing voltage steps before and during extracellular perfusion of ivabradine. We found that 30 μM ivabradine was required to achieve a ∼90% block of I_f within ∼120 s of perfusion, consistent with its half-maximal inhibitory concentration (IC_{50}) of ∼3 μM and the intracellular site of action (36, 38–40) (Fig. 1 A and B and SI Appendix, Table S1).* In current-clamp experiments, we found that 30 μM ivabradine reduced the AP-firing rate by ∼50% within 30 s of perfusion (SI Appendix, Fig. S1; P < 0.0001) and completely stopped spontaneous APs within 120 s of perfusion in most (10 of 12) cells.

Given previous reports of off-target actions of ivabradine (26, 34, 35), we next asked whether 30 μM ivabradine blocked an appreciable fraction of Ca^{2+} and K^+ currents in SAMs under our recording conditions. Ca^{2+} currents were recorded in cesium-based solutions before and after perfusion of 30 μM ivabradine (Fig. 1C). The total whole-cell Ca^{2+} current was elicited using depolarizing voltage steps from a holding potential of –90 mV. L-type Ca^{2+} current was then measured in the same cells from a holding potential of –60 mV, at which T-type Ca^{2+} currents are mostly inactivated in SAMs (24, 41). We found that 30 μM ivabradine significantly reduced total and L-type Ca^{2+} currents, blocking 30 to 40% of peak current at 0 mV (Fig. 1D and SI Appendix, Table S1). T-type Ca^{2+} current was estimated in each cell by subtracting the L-type from the total Ca^{2+} current. Ivabradine had no significant effect on the calculated T-type current (SI Appendix, Table S1). We found that 30 μM ivabradine also blocked a significant fraction of both the transient and steady-state K^+ currents (∼46 and 32%, respectively, measured by a step to +40 mV from a holding voltage of –50 mV; Fig. 1 E and F and SI Appendix, Table S1).
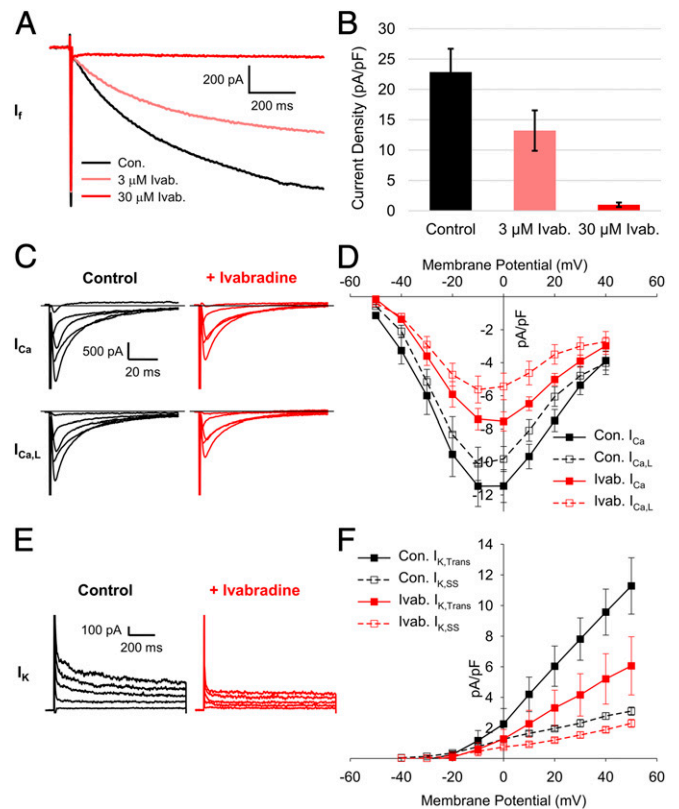
Fig. 1. A concentration of 30 μM ivabradine blocks Ca^{2+} and K^+ currents in SAMs. (A) Representative whole-cell currents recorded from a murine SAM in response to 1-s hyperpolarizing voltage steps to –130 mV from a holding potential of –60 mV in a control Tyrode's solution with 1 mM $BaCl_2$ (black) and after perfusion of Tyrode's containing 3 μM (pink) or 30 μM (red) ivabradine. (B) Average (± SEM) current density of I_f in 1 mM $BaCl_2$ (black) and after perfusion of 3 μM (pink) or 30 μM (red) ivabradine during pulses to –130 mV in murine SAMs. (C) Representative total (Top) and L-type (Bottom) whole-cell Ca^{2+} currents recorded from sinoatrial myocytes in control (black) and after perfusion of 30 μM ivabradine (red). (D) Mean (± SEM) total (closed) and L-type (open) Ca^{2+}-current density in control and after perfusion of 30 μM ivabradine using the same color scheme as C. (E) Representative whole-cell K^+ currents in a SAMs in control conditions (black) and after perfusion of 30 μM ivabradine (red). (F) Average (± SEM) transient (closed) and steady-state (open) K^+-current density in control conditions and after perfusion of 30 μM ivabradine using the same color scheme as E. Horizontal lines indicate zero current. Number of replicates and details of statistical tests can be found in SI Appendix, Table S1.

The above data indicate that ivabradine-sensitive currents in SAMs under physiological ionic conditions will include significant components of voltage-gated Ca^{2+} and K^+ currents, particularly at more depolarized potentials. Thus, we next sought to define a series of blockers that could be used to preblock Ca^{2+} and K^+ currents without affecting I_f, so that subsequent application of ivabradine could be used to isolate I_f. We measured Ca^{2+} currents before and after perfusion of 3 μM Ca^{2+}-channel blocker isradipine (Fig. 2A). As expected, 3 μM isradipine blocked most (∼90%) of the peak total and L-type Ca^{2+} currents (Fig. 2B and SI Appendix, Table S2). K^+ currents were effectively inhibited by a mixture of K^+ channel blockers (10 mM tetraethylammonium [TEA], 1 mM barium, and 1 μM E4031) followed by the same solution also containing 30 μM ivabradine (Fig. 2C). When ivabradine was applied after the K^+ channel blockers, it had almost no effect on the peak transient K^+ current and produced a small (but not significant) reduction of the steady-state K^+ current that remained in the mixture of K^+-channel blockers (Fig. 2D and SI Appendix, Table S2).
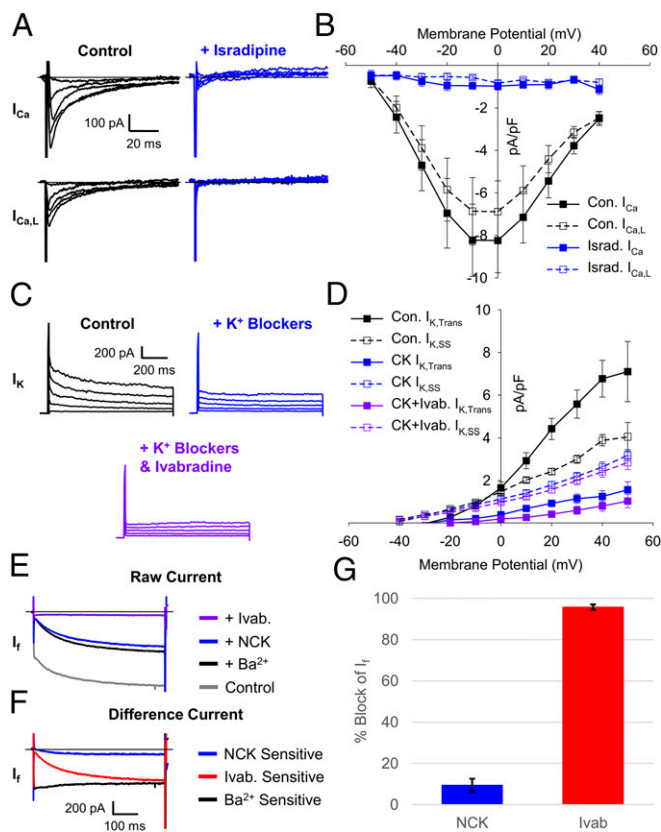
Fig. 2. The NCK cocktail blocks ivabradine off target effects but not I_f. (*A*) Representative total (*Top*) and L-type (*Bottom*) whole-cell Ca^{2+} currents recorded from SAMs in control (black) and after perfusion of 3 μM isradipine (blue). (*B*) Mean (± SEM) total (closed) and L-type (open) Ca^{2+}-current density in control and after perfusion of 3 μM isradipine using the same color scheme as *B*. (*C*) Representative K^+ currents in a SAM recorded in control conditions (black) after perfusion of a K^+ channel–blocker cocktail (1 mM $BaCl_2$, 10 mM TEA, and 3 μM E-4031; blue) and after subsequent perfusion of the K^+ channel–blocker cocktail plus 30 μM ivabradine (purple). (*D*) Average (± SEM) transient (closed) and steady-state (open) K^+-current density in control conditions after perfusion of a K^+ channel–blocker cocktail and after subsequent perfusion of 30 μM ivabradine and a K^+ channel–blocker cocktail using the same color scheme as *C*. (*E*) Representative currents recorded from a murine SAM in response to hyperpolarizing voltage steps to −130 mV from a holding potential of −60 mV in Tyrode's solution (gray), in Tyrode's after application of 1 mM barium (black), the NCK-blocker cocktail (blue), or the NCK cocktail with 30 μM ivabradine (purple). (*F*) Representative difference currents sensitive to 1 mM barium compared to control (black), NCK cocktail compared to barium alone (blue), and the NCK cocktail with 30 μM ivabradine compared to the NCK cocktail alone (red). (*G*) Average (± SEM) fraction of I_f blocked by the NCK cocktail (blue) or the NCK cocktail with 30 μM ivabradine (red) during pulses to −130 mV in murine SAMs. Horizontal lines indicate zero current. Number of replicates and details of statistical tests can be found in *SI Appendix*, Table S2.

To determine whether the Ca^{2+}- and K^+-channel blockers had any effect on I_f, we next applied them together with the Na^+-channel blocker tetrodotoxin (TTX; 30 μM) to isolated SAMs (Fig. 2 *E* and *F*). A concentration of 30 μM TTX was included in our preblock mixtures because ivabradine has previously been shown to block Na^+ currents (26), and 30 μM TTX inhibits both weakly TTX-sensitive Nav1.5 channels as well as highly TTX-sensitive Nav1.1 channels expressed in the murine sinoatrial node (42, 43). We found that the Na^+-Ca^{2+}-K^+ (NCK) channel–blocker cocktail blocked ~10% of the inward current that was activated during 1-s hyperpolarizations to −120 mV (Fig. 2 *E* and *G* and *SI Appendix*, Table S2); however, the I_f amplitude after perfusion of the NCK cocktail did not differ significantly from the current after application

of only the inward rectifier K^+-channel blocker, barium (*SI Appendix*, Table S2), which has long been used to isolate I_f (21, 44). This indicates that TTX, isradipine, TEA, and E4031 exhibit no additional block of I_f. Subsequent addition of 30 μM ivabradine to the NCK cocktail significantly blocked I_f by ~95% compared to barium alone (Fig. 2 *E* and *G* and *SI Appendix*, Table S2). Thus, the NCK-blocker cocktail containing TTX, isradipine, TEA, barium, and E4031 can be used to effectively preblock the off-target effects of ivabradine on Na^+, Ca^{2+}, and K^+ currents in SAMs, with minimal effects on I_f.

I_f Flows Both Inward and Outward during the Cardiac Cycle in SAMs. Having identified conditions for pharmacological isolation of I_f in SAMs, we next used the AP-clamp technique to record the native I_f flowing in response to APs recorded from the same cell. The experimental approach is illustrated in *SI Appendix*, Fig. S2. In each cell, we first recorded spontaneous APs in current-clamp mode without current injection in the presence of either 1 nM (control) or 1 μM (stimulated) of the β-AR agonist, isoproterenol. As expected, the AP-firing rate was significantly faster in 1 μM isoproterenol compared to 1 nM isoproterenol (*SI Appendix*, Table S3). From each of these recordings, a representative 10-s train of APs was integrated into a voltage protocol, which appended square voltage steps to the end of the train of APs so that the degree of the drug block could be monitored. Finally, repeated sweeps of the cell-specific AP-clamp voltage protocol were applied to each cell in voltage-clamp mode to elicit currents in a series of different solutions.

In each cell, AP-elicited currents were first recorded in the absence of blockers (but in the presence of 1 nM or 1 μM isoproterenol), then in response to wash-on of the NCK cocktail, and finally upon wash-on of the NCK cocktail plus 30 μM ivabradine (Fig. 3 *A* and *B*). AP-elicited currents were analyzed in the last 2 s of each train of APs, at which point I_f is no longer influenced by the interpulse holding potential between AP trains. I_f was defined in these experiments as the ivabradine-sensitive difference current, which was calculated by subtracting the current after application of 30 μM ivabradine in the presence of the NCK cocktail from the current in the NCK cocktail alone (Fig. 3 *A* and *B*).

I_f was evident as both an inward current at diastolic potentials and an outward current during the AP upstroke and repolarization phases. In the control condition of 1 nM isoproterenol, the inward component of the ivabradine-sensitive current peaked at an average of −18 pA, and the outward current peaked at 29 pA (*SI Appendix*, Table S3). As expected, 1 μM isoproterenol reduced the cycle length, which decreased the time for I_f activation during the diastolic depolarization. Nonetheless, 1 μM isoproterenol significantly increased the peak inward I_f density during the AP. Thus, the depolarizing shift in voltage dependence, the accelerated activation rate, and the slowed deactivation rate of I_f in response to β-AR stimulation are more than sufficient to overcome the decreased time for channel activation at faster AP-firing rates (Fig. 3*C* and *SI Appendix*, Table S3). Outward currents in 1 μM isoproterenol also tended to be larger than those in 1 nM isoproterenol (Fig. 3*C*), although the difference did not reach statistical significance.

Unfortunately, the inhibition of the potassium current by the blocker cocktail was incomplete in three cells. To increase the resolution of I_f in the absence of this contamination of the ivabradine-sensitive I_f with the K^+ current, we confined the analysis of I_f to cells in which ivabradine had no effect on the steady-state potassium current remaining in the blocker mixture (*Materials and Methods* and *SI Appendix*, Fig. S3). In cells included in the analysis, the reversal potential of the ivabradine-sensitive current did not differ from the reversal potential of steady-state I_f elicited by hyperpolarizing voltage steps in SAMs in 1 nM or 1 μM isoproterenol (Fig. 3*D* and *SI Appendix*, Table S3; $P = 0.5125$).

We next examined the correlation between the inward and outward ivabradine-sensitive currents by comparing their rates of
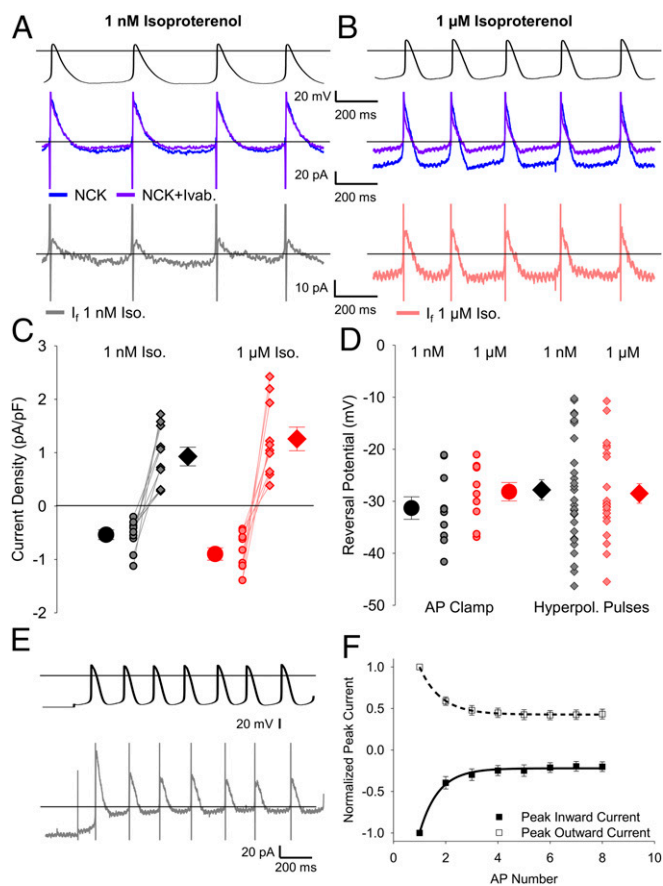
www.manaraa.com

PHYSIOLOGY

Fig. 3. I_f flows both inward and outward during sinoatrial APs. (*A* and *B*) Representative whole-cell currents (*Middle*) elicited by APs recorded from the same cell (*Top*) after the addition of the NCK cocktail (blue) or the NCK cocktail plus 30 μM ivabradine (purple). (*Bottom*) The ivabradine-sensitive I_f difference current was determined as the current in the NCK cocktail plus ivabradine minus the current in the NCK cocktail alone in 1 nM isoproterenol (gray) or 1 μM isoproterenol (pink). (*C*) Average (± SEM) peak inward (circles) and outward (diamonds) I_f current density in 1 nM isoproterenol (black) and 1 μM isoproterenol (red). Individual recordings in 1 nM isoproterenol (gray) or 1 μM isoproterenol (pink) are shown using the smaller symbols. (*D*) Average (± SEM) reversal potential for ivabradine-sensitive current in 1 nM and 1 μM isoproterenol measured during AP waveforms (circles) and hyperpolarizing pulses (diamonds) using the same color scheme as *C*. Number of replicates and details of statistical tests can be found in *SI Appendix*, Table S3. (*E*) Representative ivabradine-sensitive currents (*Bottom*) in a sinoatrial myocyte in response to APs following a holding potential of −70 mV (*Top*) in 1 nM isoproterenol. (*F*) Average (± SEM) peak inward (closed) and peak outward (open) currents recorded in SAMs during the first 8 APs after holding at −70 mV in 1 nM isoproterenol (*n* = 7). Average time courses were fit by a single exponential equation and are normalized to the peak current during the first AP in the same cell. The comparison of the time constants for inward and outward current decay was performed with a paired *t* test (*P* = 0.7790). Horizontal lines indicate zero voltage or zero current levels.

change at the initiation of a train of APs that was given following a holding potential of −70 mV (Fig. 3*E*). The relatively negative holding potential partially activated I_f before the train of APs, allowing us to measure the time courses of decay in the peak outward and inward currents simultaneously, as I_f deactivated to a new smaller steady-state level at the start of the train of APs. We found that the inward and outward ivabradine-sensitive currents decayed at similar rates (Fig. 3*F*; 200.4 ± 50.9 ms, *n* = 6 for inward; 191.4 ± 29.4 ms, *n* = 6 for outward; *P* = 0.7790), consistent with their common origin from I_f channels with relatively slow relaxation kinetics as membrane voltage is changed. Overall, these data establish that

I_f is active during both the diastolic depolarization and repolarization phases of the sinoatrial AP.

Current–Voltage Relationships of Ivabradine-Sensitive Current during the Cardiac Cycle in SAMs. To further probe the attributes of the ivabradine-sensitive current, we next examined its current–voltage relationships. For each cell, the ivabradine-sensitive current was plotted as a function of the voltage of the AP command waveform. Current–voltage relationships were averaged for four consecutive APs (capacitive transients, which represent ∼1 ms of data during the AP upstroke, were eliminated). We found that the current–voltage relationships for the ivabradine-sensitive current in both 1 nM and 1 μM isoproterenol were fairly linear at more negative potentials (Fig. 4*A*). The slope of the outward component of the current–voltage relationship was somewhat steeper than that of the inward component in many cells, perhaps reflecting the slight outward rectification of fully activated I_f previously described (21, 45, 46). In some cells, there may also be a small amount of contamination of the outward current by an ivabradine-sensitive outward current not fully blocked by the NCK cocktail (*SI Appendix*, Fig. S3*A*).

The close tracking of the ivabradine-sensitive current to the AP waveform (Fig. 3 *A* and *B*) and the fairly linear current–voltage relationships (Fig. 4*A*) suggest that I_f undergoes little voltage-dependent gating during the cardiac cycle in SAMs. To estimate the changes in I_f gating during the cardiac cycle, we compared the current amplitude at −60 mV during the latter part of the diastolic depolarization (just prior to the AP upstroke) to the current at −60 mV during the latter part of the AP repolarization (just after the AP downstroke) (Fig. 4 *B*, *Inset*). We chose −60 mV as a test potential for these comparisons because it is sufficiently hyperpolarized relative to the reversal potential to allow accurate measurement of the small ivabradine-sensitive current and because it precedes the capacitive transient. We found that, despite the variable cycle lengths of the APs in our dataset, the average current amplitudes at −60 mV in SAMs did not differ significantly between the depolarization and repolarization phases in either 1 nM or 1 μM isoproterenol (Fig. 4*B* and *SI Appendix*, Table S3), and differences in current amplitude in individual cells were not correlated to AP firing rate (*P* = 0.4220). These data are consistent with the idea that there is little or no voltage-dependent gating of I_f during the AP in SAMs.

I_f Contributes Substantially to the Net Current during Both the Diastolic Depolarization and Repolarization Phases of the AP. We next estimated the contribution of I_f to the net inward and outward charge movement during the sinoatrial AP. The net current in each cell during the AP was calculated as the first derivative of membrane potential scaled by capacitance. For I_f, we extrapolated a linear fit to the I_f current–voltage relationship negative to −20 mV as a conservative estimate of the magnitude of outward I_f in the absence of any potential contamination (*SI Appendix*, Fig. S4 *A* and *B*). Comparison of I_f to the net current showed that I_f comprises a substantial fraction of the net charge moved during the sinoatrial AP. In 1 nM isoproterenol, I_f contributed 1.6 ± 0.35 pC (*n* = 10) of inward charge and 0.2 ± 0.05 pC (*n* = 10) of outward charge throughout each AP cycle (Fig. 5*A* and *SI Appendix*, Table S3). Importantly, this represents 50.2 ± 10.1% (*n* = 10) and 6.6 ± 1.9% (*n* = 10) of the net inward and outward charge movement, respectively (Fig. 5*B*). When compared to the ∼30 pF average cellular capacitance (*SI Appendix*, Table S3), the ivabradine-sensitive I_f alone would be sufficient to depolarize the membrane by 45 mV and to repolarize the membrane by 6 mV during each AP in the absence of other conductances. Despite a shorter AP cycle length that decreases the amount of time I_f has to activate and to pass charge during each AP, 1 μM isoproterenol increased the inward charge density moved by I_f by ∼40% (*SI Appendix*, Table S3), more than doubled the rate of inward charge movement (*SI Appendix*, Table S3),
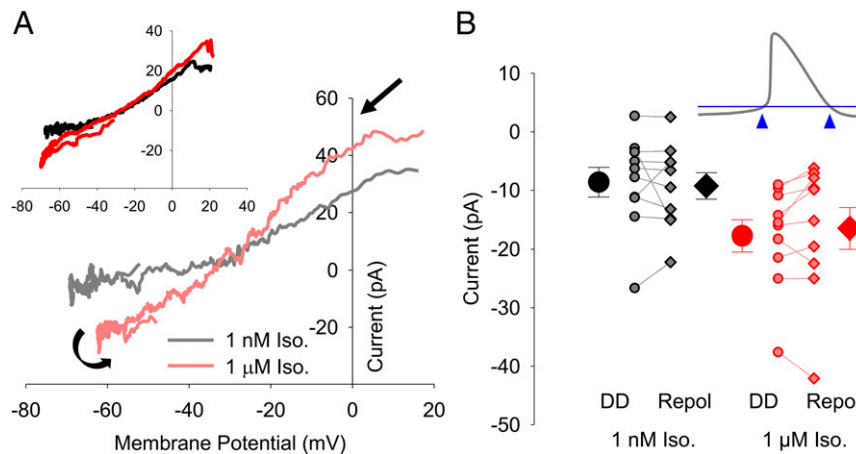
Fig. 4. Current–voltage relationships and limited gating of I_f in SAMs. (A) Representative current–voltage relationships of ivabradine-sensitive I_f from single cells in 1 nM isoproterenol (gray) or 1 μM isoproterenol (pink). Black arrows indicate the progression of the current–voltage relationship over time. (A, Inset) Averaged current–voltage relationships of ivabradine-sensitive I_f in 1 nM isoproterenol (n = 10; black) or 1 μM isoproterenol (n = 10; red). (B) Average (± SEM) I_f current amplitude recorded at −60 mV during the diastolic depolarization (DD; circles) and following AP repolarization (Repol; diamonds) in 1 nM isoproterenol (black) and 1 μM isoproterenol (red). Individual recordings in 1 nM isoproterenol (gray) or 1 μM isoproterenol (pink) are shown using the smaller symbols. (B, Inset) Schematic showing points at which I_f was measured in panel B. Number of replicates and details of statistical tests can be found in *SI Appendix*, Table S3.

and increased I_f as a fraction of the net inward current to 93.4 ± 16.0% (Fig. 5B; P = 0.0353). In 1 μM isoproterenol, I_f contributes enough charge to depolarize the membrane by 85 mV. Application of 1 μM isoproterenol had no significant effect on outward ivabradine-sensitive charge movement, which remained at about 7% of the net charge. Although the rate of outward charge movement in 1 μM isoproterenol was nearly double that in 1 nM isoproterenol, this difference was also not statistically significant (*SI Appendix*, Table S3). We suspect the lack of significant differences in both the outward currents and charge movement are due to the large variability in the peak potential during depolarization which, in turn, increases the variability of the outward driving force and, consequently, the outward current densities (Fig. 3C). Ultimately, these data show that I_f contributes substantially to the charge movement during both the diastolic depolarization and repolarization phases of the sinoatrial AP. Furthermore, the β-AR–driven increase in the fraction of inward charge movement attributable to I_f strongly suggests that I_f contributes to the β-AR increase in AP-firing rate.

Limited Voltage-Dependent Gating of HCN4 Channels in HEK Cells in Response to Sinoatrial APs. To better resolve the properties of I_f during the sinoatrial AP, we next recorded currents passed by HCN4 channels expressed in HEK293 cells in response to APs recorded from SAMs (Fig. 6 and *SI Appendix*, Table S4). Control APs recorded in 1 nM isoproterenol were used to evoke HCN4-mediated current in HEK cells without 3',5'-cyclic adenosine monophosphate (cAMP) in the pipette, and APs recorded in 1 μM isoproterenol were used in HCN4-expressing HEK cells in which cAMP was present. Whole-cell currents were recorded before and after perfusion of 30 μM ivabradine in the presence of Ca^{2+}- and K^+-channel blockers (to block any endogenous currents in HEK cells) and in either the absence (Fig. 6A) or presence (Fig. 6B) of 1 mM cAMP in the recording pipette. The HCN4-generated current was determined as the ivabradine-sensitive difference current. In agreement with the above data from SAMs, HCN4 currents elicited by sinoatrial APs closely tracked the shape of the AP and had both inward and outward components (Fig. 6 A and B). When plotted against the membrane potential, the HCN4 current was roughly linear throughout the duration of the AP, with slight outward rectification (Fig. 6C). As expected, inclusion of 1 mM cAMP in the recording pipette significantly increased the inward and outward current densities during the AP and the slope of the current–voltage relationship (Fig. 6C and *SI Appendix*, Table S4). Importantly, HCN4 currents in HEK cells exhibited little voltage-dependent gating
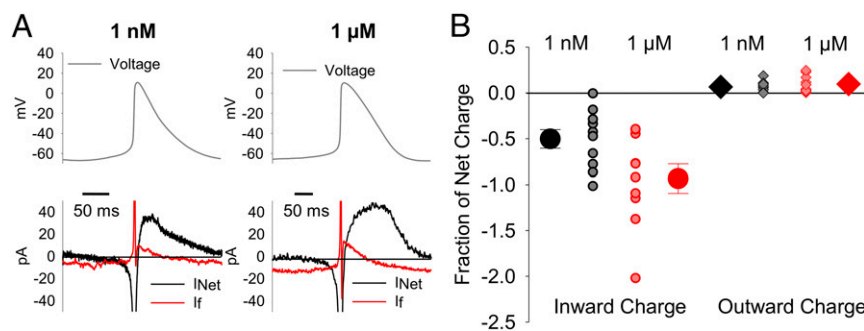

Fig. 5. I_f contributes substantial inward and outward charge movement during the SAM AP. (A) Representative calculated net current (black) and measured ivabradine-sensitive I_f (red) during a single sinoatrial AP (Top) in 1 nM isoproterenol or in 1 μM isoproterenol. Horizontal lines indicate zero current. (B) Average (± SEM) ivabradine-sensitive inward (circles) and outward (diamonds) charge movement as a fraction of the net charge during a single AP in 1 nM (black) and 1 μM (red). Individual recordings in 1 nM isoproterenol (gray) or 1 μM isoproterenol (pink) are shown using the smaller symbols. Number of replicates and details of statistical tests can be found in *SI Appendix*, Table S3.
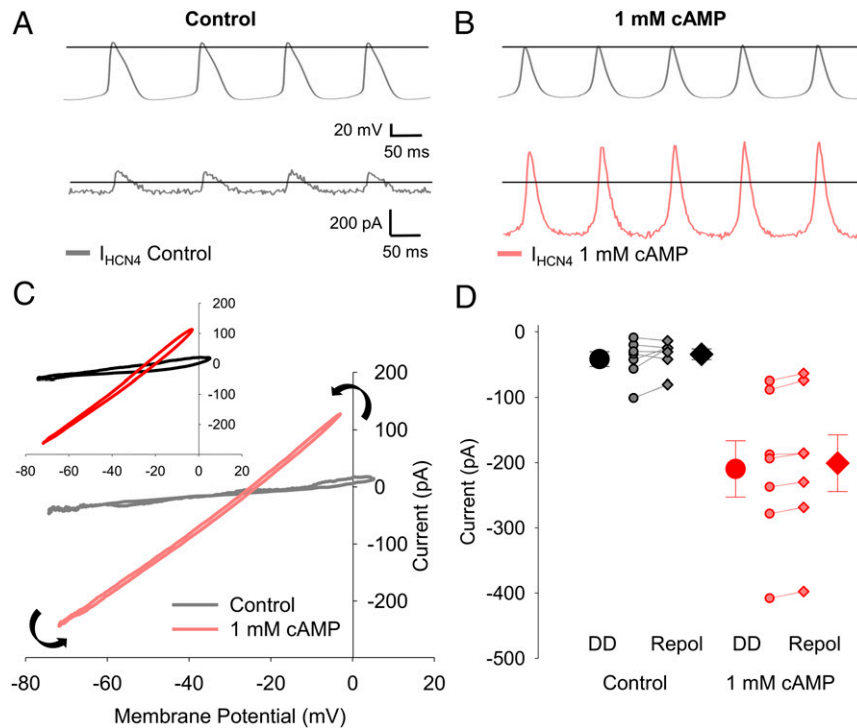
Peters et al.
Bidirectional flow of the funny current (If) during the pacemaking cycle in murine sinoatrial node myocytes

PNAS | 5 of 12
https://doi.org/10.1073/pnas.2104668118

www.manaraa.com

Fig. 6. HCN4 channels in HEK cells pass a biphasic current with limited voltage-dependent gating in response to sinoatrial APs. (*A*) Representative ivabradine-sensitive HCN4 current in the absence of cAMP (gray) recorded from a HEK cell in response to APs recorded from a SAM in 1 nM isoproterenol (*Top*). (*B*) Representative ivabradine-sensitive HCN4 current with 1 mM cAMP in the intracellular solution (pink) recorded in a HEK cell in response to APs recorded from a SAM in 1 μM isoproterenol (*Top*). Horizontal lines indicate zero voltage or zero current levels. (*C*) Representative current–voltage relationships of ivabradine-sensitive HCN4 currents in control (gray) or 1 mM cAMP (pink). Black arrows indicate the progression of the current–voltage relationship over time. (*C, Inset*) Average current–voltage relationships of ivabradine-sensitive HCN4 currents in control (black) and 1 mM cAMP (red). (*D*) Average (± SEM) HCN4 current amplitude recorded at −60 mV during the latter diastolic depolarization (DD; circles) and AP repolarization (Repol; diamonds) in control (black) and 1 mM cAMP (red). Individual recordings in control (gray) or 1 mM cAMP (pink) are shown using smaller symbols. Number of replicates and details of statistical tests can be found in *SI Appendix*, Table S4.

during the AP; the current–voltage relationships during the up-stroke and repolarization phases of the AP were similar (Fig. 6*C*). Ivabradine-sensitive currents in HEK cells at −60 mV prior to the AP upstroke did not significantly differ from those measured at −60 mV during the AP downstroke in the absence of cAMP (Fig. 6*D* and *SI Appendix*, Table S4). With 1 mM cAMP in the pipette, the current measured at −60 mV following repolarization was slightly (<5%) reduced in most cells compared to the current during the depolarization phase, consistent with a small amount of deactivation during the AP (Fig. 6*D* and *SI Appendix*, Table S4). These results in HEK cells are in good agreement with our findings that native I_f passes substantial inward and outward current in response to the AP in SAMs and that less than 5% of open channels deactivate during the AP.

Slow Activation and Deactivation of HCN4 Underlies Limited Gating during the Sinoatrial AP. To further corroborate our findings from SAMs and to investigate the biophysical properties of I_f that contribute to its persistent activation throughout the AP cycle in SAMs, we next used mathematical modeling to simulate I_f during the sinoatrial AP. We refined an existing model of I_f (47) to fit the currents elicited by square-wave hyperpolarizing voltage protocols in murine SAMs in either 1 nM or 1 μM isoproterenol (*SI Appendix*, Fig. S5). Sets of APs recorded from multiple cells in either 1 nM (n = 10) or 1 μM (n = 10) isoproterenol were then used to stimulate the models. For each simulation, the conductance of I_f in the model was scaled to match the I_f current measured in the cell from which the APs were recorded.

Although the simulated steady-state current–voltage relationships showed little current at potentials corresponding to the diastolic depolarization (*SI Appendix*, Fig. S5*C*), both models produced currents during the AP, with inward and outward components (Fig. 7 *A* and *B*) similar to those recorded from SAMs and HCN4-expressing HEK cells (Figs. 3 and 6). Simulated currents produced by the 1 μM model were larger than those produced by the 1 nM model (Fig. 7 *C, Inset* and *D* and *SI Appendix*, Table S5), and this difference in current amplitude persisted when the models were scaled to the same maximum conductance (*SI Appendix*, Fig. S6*A*), consistent with experimental observations that isoproterenol increases I_f amplitude primarily through changes to gating and not maximal conductance (21, 48, 49). The 1 nM model exhibited little voltage-dependent gating as assessed by similar current–voltage relationships during the upstroke and downstroke (Fig. 7*C*) and similar current amplitudes at −60 mV before and after the AP (Fig. 7*D* and *SI Appendix*, Table S5), consistent with the data acquired in SAMs and HCN4-expressing HEK cells (Figs. 4 and 6). However, the 1 μM isoproterenol model displayed a limited amount of gating by both measures, primarily in simulations with APs that had a more negative maximum diastolic potential or larger AP amplitude (Fig. 7 *C* and *D*). Importantly, when the sets of APs used to stimulate the models were swapped, the current–voltage relationships remained relatively linear (*SI Appendix*, Fig. S6*B*), further indicating that changes in the AP cycle length have minimal effects on the fraction of channels that activate/deactivate during each cycle. Overall, these simulations corroborate our findings that the majority (>80%) of open channels remain open throughout the entirety of the sinoatrial AP.
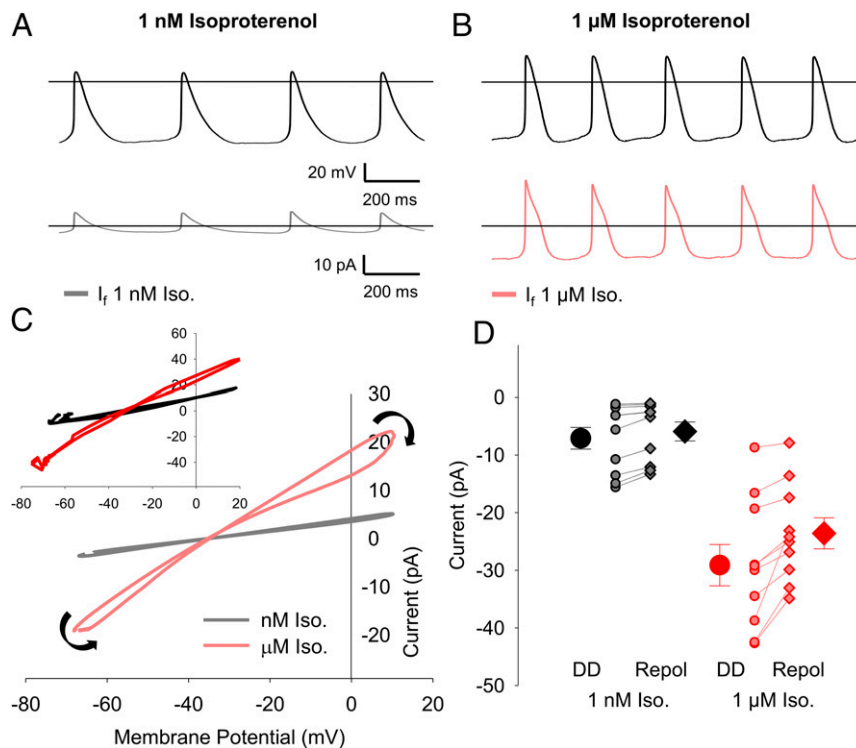
Fig. 7. Simulations of I_f produce a biphasic current with limited voltage-dependent gating in response to sinoatrial APs. (*A*) Simulated I_f generated by a model fit to data from 1 nM isoproterenol (gray) in response to APs recorded in 1 nM isoproterenol (*Top*). (*B*) Simulated I_f generated by a model fit to data from 1 μM isoproterenol (pink) in response to APs recorded in 1 μM isoproterenol (*Top*). Horizontal lines indicate zero voltage or zero current levels. (*C*) Representative current–voltage relationships of I_f simulated by the 1 nM model (gray) or the 1 μM model (pink) in response to sinoatrial APs recorded from single cells in the same condition. Black arrows indicate the progression of the current–voltage relationship over time. (*C, Inset*) Average current–voltage relationships of I_f simulated by the 1 nM model (black) or the 1 μM model (red) in response to the full sets of sinoatrial APs recorded in 1 nM or 1 μM isoproterenol. (*D*) Average ($\pm$ SEM) simulated I_f current amplitude at −60 mV during the latter diastolic depolarization (DD; circles) and AP repolarization (Repol; diamonds) in response to recorded sinoatrial APs simulated using the 1 nM isoproterenol model (black) or the 1 μM isoproterenol model (red). Individual simulations in response to different 1 nM (gray) or 1 μM (pink) APs are shown by the smaller symbols. Number of replicates can be found in *SI Appendix*, Table S5.

We hypothesized that the lack of appreciable gating of I_f during the AP is caused by the relatively slow rates of activation and deactivation of the sinoatrial HCN4 isoform compared to the faster gating of neuronal HCN1 and HCN2 channels. To test this hypothesis, we compared the response of the 1 nM model of I_f to those of previously published models of HCN1 (50) and HCN2 (51), which activate and deactivate up to an order of magnitude more rapidly than HCN4 (6, 52–56). Compared to HCN4, which activates with a time constant of ~450 ms at −140 mV, HCN1- and HCN2-activation time constants at −140 mV are ~30 ms and ~184 ms, respectively (6). Similarly, at −50 mV, the deactivation time constants in HCN1 and HCN2 (~125 ms and ~600 ms, respectively) are far more rapid than that of HCN4 (~1.6 s) (17). In contrast to the 1 nM I_f model, both the HCN1 and HCN2 models showed prominent activation during the AP cycle as seen by figure-eight shaped current–voltage relationships (Fig. 8*A*). Indeed, the HCN1 model, which has the fastest kinetics and most depolarized voltage dependence, completely deactivated during the AP upstroke and contributed little outward current during the AP-repolarization phase. HCN2, which has activation and deactivation rates more similar to those of HCN4, showed considerable outward current during the upstroke but was mostly deactivated during the AP downstroke.

To elucidate how the individual gating parameters impact the current–voltage relationships of I_f, we compared the base 1 nM I_f model to the 1 nM model in which the three individual components of the model were changed independently (voltage-dependent activation, the forward rate (α) of the activation transition, and the

reverse rate (β) of the activation transition (Fig. 8 *B–D*)). We found that 5 mV depolarizing or hyperpolarizing shifts in the voltage dependence of activation or a 15 mV depolarizing shift corresponding to stimulation by 1 μM isoproterenol primarily increased or decreased the slope of the current–voltage relationship without much change in the amount of deactivation during the AP (~15 to 20% in all cases; Fig. 8*B*). In contrast, a model in which the forward rate was sped up by 50 times led to prominent I_f activation during the diastolic depolarization (Fig. 8*C*), and a model with the reverse rate sped up 50 times showed both I_f activation during the diastolic depolarization and I_f deactivation during the AP upstroke and repolarization phases (Fig. 8*D*), similar to that seen in the HCN1 and HCN2 models (Fig. 8*A*). Changing the α- and β-rates of the 1 nM model to those in the 1 μM model or slowing them by 50× did not substantially alter channel gating during the AP and only modestly altered the slope of the current–voltage relationship (Fig. 8 *C* and *D*). Overall, these data show that the steady-state voltage-dependent activation of I_f is the primary determinant of the slope of the current–voltage relationship but plays little role in the degree of activation and deactivation gating during the AP. In contrast, the persistent activation of I_f during the sinoatrial AP and the resulting linear current–voltage relationship appear to be mainly determined by the slow activation and deactivation rates of the underlying HCN4 channels.

Discussion

Despite decades of research dedicated to defining the ionic currents that underlie cardiac pacemaking in SAMs, little consensus has emerged on how I_f contributes to the generation of spontaneous
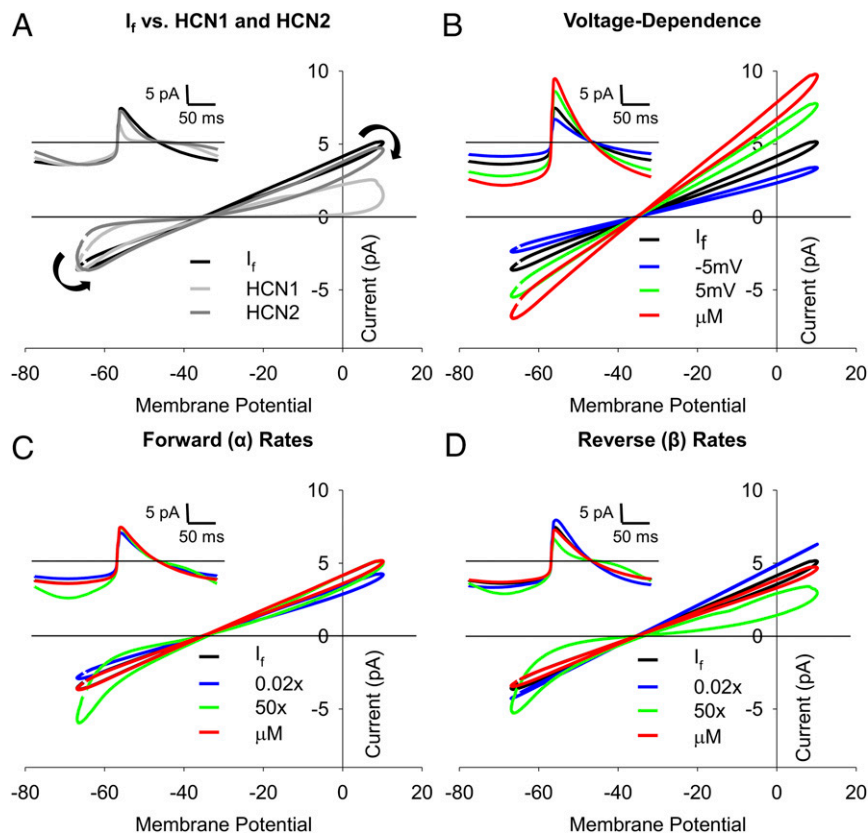
Peters et al.
Bidirectional flow of the funny current (I_f) during the pacemaking cycle in murine sinoatrial node myocytes

PNAS | 7 of 12
https://doi.org/10.1073/pnas.2104668118

www.manaraa.com

Fig. 8. Linear I_f current–voltage relationships are due to slow activation and deactivation rates. (*A*) Simulated current–voltage relationships in response to a representative sinoatrial AP recorded in 1 nM isoproterenol using the base 1 nM isoproterenol model of I_f (black), a model of HCN1 (light gray) (50), or a model of HCN2 gating (dark gray) (51). Black arrows indicate the progression of the current–voltage relationship over time. (*A*, *Inset*): Simulated currents during single sinoatrial APs using the base 1 nM isoproterenol model of I_f, the HCN1 model, or the HCN2 model. (*B*–*D*) Current–voltage relationships of simulated I_f in response to prerecorded sinoatrial APs using the base 1 nM isoproterenol model (black), the 1 μM isoproterenol model (red), or the 1 nM model with altered activation voltage dependence (*B*), forward (α) rates of activation (*C*), or reverse (β) rates of activation (*D*). Activation voltage dependence ($V_{1/2}$) was shifted by −5 mV (blue) or +5 mV (green). The α- and β-rates of the activation gate were slowed by 50× (blue) or sped up 50× (green). (*B*–*D*, *Insets*) Simulated I_f during single sinoatrial APs using the base 1 M isoproterenol model, the 1 μM isoproterenol model, or models with altered activation voltage dependence (*B*, *Inset*), α-rates (*C*, *Inset*), or β-rates (*D*, *Inset*). Color schemes in *B*–*D*, *Insets* are the same as the main panels. Horizontal lines indicate zero current.

APs (9, 12, 57, 58). We here establish a new conceptual framework for the role of I_f as a driver of oscillatory electrical activity in SAMs by showing that it flows both inward and outward during the AP. Our results specifically reveal the following: 1) I_f is active throughout the sinoatrial AP and passes both inward and outward current; 2) I_f contributes a substantial portion of the net depolarizing and repolarizing charge movement during the sinoatrial AP; 3) β-AR stimulation increases the fraction of net depolarizing charge contributed by I_f consistent with a contribution to the fight-or-flight increase in heart rate; 4) there is limited voltage-dependent gating of I_f during the cardiac cycle in SAMs; and 5) the slow rates of activation and deactivation of the sinoatrial HCN4 channel isoform contribute to the persistent activation of I_f throughout the cardiac cycle in SAMs.

I_f in SAMs Drives Membrane Potential Oscillations in Both Directions during the AP. Most studies of I_f have focused on its role as an inward current during the diastolic depolarization phase of the sinoatrial AP (9, 12, 14–16). While mathematical models and some previous studies have suggested that I_f may also conduct outward current in SAMs (18–20, 59, 60), our experimental data conclusively demonstrate that I_f is active throughout the entire AP cycle (Figs. 3–5). This behavior was confirmed in AP-clamp recordings of HCN4-mediated currents in HEK cells (Fig. 6) and AP-clamp simulation of a mathematical model of I_f parameterized using

traditional square-wave protocols (Fig. 7). Together, the data indicate that I_f serves a critical role in the generation of spontaneous activity in the cardiac pacemaker by driving membrane potential oscillations in both directions. It follows that I_f must contribute to shaping both the diastolic depolarization and repolarization phases of the sinoatrial AP. This unique function of I_f arises as a result of both its reversal potential and its slow kinetics; the reversal potential of ∼ −30 mV confers driving force at both extremes of the voltage excursion of the sinoatrial AP (roughly −60 to +10 mV), while the slow rates of activation and deactivation conspire to keep the hyperpolarization-activated channels open throughout the entire AP cycle.

Limited Voltage-Dependent Gating Due to Slow Kinetics of HCN4. Strikingly, our data show that there is little voltage-dependent activation or deactivation of I_f during the cardiac cycle in SAMs, either at resting AP-firing rates (in 1 nM isoproterenol) or at the higher firing rates seen in response to β-AR stimulation (in 1 μM isoproterenol). The lack of appreciable gating was recapitulated by heterologously expressed HCN4 channels and by mathematical models of I_f (Figs. 6 and 7). Our subsequent modeling (Fig. 8) suggested that the voltage-independent nature of I_f recorded in AP-clamp experiments is mainly determined by the intrinsically slow rates of activation and deactivation of HCN4 compared to other HCN isoforms. Our findings help resolve the paradox of

how such a slowly activating current can contribute to the diastolic depolarization of sinoatrial cells (12, 13) by showing that the equally slow deactivation rate results in a conductance that is activated throughout the entirety of the AP cycle.

An important consequence of this persistent activation is that I_f contributes a substantial fraction of the total charge movement in SAMs that belies its relatively small peak current amplitude and low open probability. Indeed, the peak amplitude of I_f during the cardiac cycle in SAMs is only ~10 to 30 pA, consistent with its negative range of voltage activation relative to the voltages of the sinoatrial AP (e.g., *SI Appendix*, Fig. S5C). These currents cause activation of only a small fraction of the total HCN channels in the cell. Based on an average maximal conductance of 11.79 nS measured during hyperpolarizing voltage steps (*SI Appendix*, Fig. S5), a maximum of ~2% of HCN channels are open during the diastolic depolarization in 1 nM isoproterenol and ~5% in 1 µM isoproterenol. Yet, despite the small peak current amplitudes and low open probability, I_f contributes 50% of the net inward charge (~3.1 pC) and 6.5% of the net outward charge (~3.1 pC) during the AP (Fig. 5B) due to its persistent activity. These results provide a mechanistic framework for numerous qualitative observations from mutation, blocker, and simulation studies that illustrate that I_f is critical for pacemaker function.

Increased I_f during Diastole Contributes to the Fight-or-Flight Response.
The lack of appreciable gating of I_f during the cardiac cycle does not mean that voltage-dependent gating of I_f is irrelevant for the physiological function of HCN4 channels. (Patho)physiological modulators of I_f, such as β-AR stimulation (3, 48), aging (24), and mutations (61) that alter the voltage dependence of I_f can change the fraction of channels that are open during the AP to modulate the AP firing rate. Indeed, our data show that the shift in voltage dependence of I_f in response to β-AR stimulation increases the fraction of open channels during the AP, yielding a new gating equilibrium with larger currents and increased charge movement throughout the AP cycle (Figs. 3–7). During β-AR stimulation, inward charge movement corresponding to I_f increases nearly 40%, driven by increased HCN4 channel open probability in response to cAMP and protein kinase A phosphorylation (Fig. 8B) (3, 62, 63). Importantly, even with the reduced time for channel activation due to the faster AP-firing rates during β-AR stimulation, I_f remains active throughout the entirety of the AP.

The persistent activation of I_f may play an important role in stabilizing AP firing in the sinoatrial node because the amount of current does not change appreciably on a beat-to-beat basis. I_f thus tends to counter variance in cycle length and AP waveform. Accordingly, knockout and knockdown of HCN4 in mice have consistently shown that I_f is necessary to stabilize basal AP firing rates in SAMs (9, 64–67) and to prevent sinus pauses (68). However, there is less consensus on the contribution of I_f to the fight-or-flight increase in heart rate. SAMs isolated from inducible knockouts of HCN4 in adult mice respond normally to isoproterenol in some lines (66, 67) but have a decreased response in others (64), and the inducible deletion of cyclic nucleotide binding via the HCN4-573X mutant reduces the exercise-induced maximal heart rate and decreases the maximal AP-firing rate of isolated cells in response to isoproterenol but does not fully eliminate β-adrenergic–stimulated increases in SAM firing rate and heart rate (65). Importantly, interpretation of these models is complicated by the presence of residual I_f, possibly due to expression of other HCN-channel isoforms (66). Furthermore, this lack of clarity regarding the contribution of I_f may reflect altered regulation of other mechanisms of heart rate regulation when HCN4 is knocked out. While our data do not imply that I_f is the only driver of the β-AR–mediated increase in heart rate, they demonstrate conclusively that β-adrenergic stimulation increases the I_f amplitude and its relative contribution to the net inward charge movement during the diastolic depolarization, consistent with a role for I_f in the fight-or-flight increase in heart rate as has long been suggested (3).

Limitations of Blockers.
Some of the historic difficulty in evaluating the role of I_f in pacemaking stems from the limitations of available blockers. For example, Cs^+ has long been used to block I_f; however, Cs^+ also blocks inward rectifier K^+ channels and alters gating of Kv11.1 (hERG) (28–30). Moreover, the Cs^+-sensitive current in SAMs underestimates I_f because Cs^+ block of inward I_f is relieved at more depolarized membrane potentials and because Cs^+ does not block outward current through HCN channels (46). Substantial off-target effects have similarly been reported for other HCN-channel blockers including ZD7288 (27, 33), zatebradine (31, 32, 36, 37), and cilobradine (32, 69). We used ivabradine in the present study, as it has relatively low arrhythmogenic potential at the therapeutic concentration of 3 µM (8, 36, 37, 70) and because it is widely used as a research tool to study HCN-channel currents in native tissues (38, 61, 65, 71, 72). However, our experiments required a fairly complete block of I_f, and we found that, at the concentration required to achieve about a 90% block of I_f in SAMs (30 µM), ivabradine exhibited substantial off-target block of voltage-gated Ca^{2+} and K^+ currents (Fig. 1). This is consistent with previous reports (26, 34, 35) and with its increased arrhythmogenic potential at higher concentrations (39). Despite the off-target effects, we were able to measure I_f as the ivabradine-sensitive current in SAMs by preblocking Na^+, K^+, and Ca^{2+} currents (Fig. 2), similar to methods used to isolate AP-elicited currents mediated by Kv3 channels in dorsal root ganglion (DRG) neurons (73) and the sequential blocker application approach used to isolate currents in ventricular myocytes (74).

To improve the resolution of the properties of I_f during the AP, three cells recorded in 1 nM isoproterenol were not included in the main analysis due to K^+-current contamination owing to incomplete perfusion by the blocker mixture as indicated by reversal potentials more negative than −50 mV (*SI Appendix*, Fig. S3B). However, inclusion or deletion of these cells has no impact on the conclusions that the inward current density (*SI Appendix*, Fig. S3C) and inward charge density are significantly smaller in 1 nM versus 1 µM isoproterenol ($P = 0.0045$ and $P = 0.0055$, respectively) and that gating is limited during the AP (*SI Appendix*, Fig. S3 C and D; $P = 0.6248$).

While our control experiments and preblock approach revealed several off-target effects of ivabradine, it is important to note that it was not feasible to inhibit all possible ivabradine-sensitive currents in SAMs, such as background currents of unknown molecular origin and the Na^+/Ca^{2+} exchanger (NCX), which is known to be critical for pacemaker activity in SAMs (75, 76). Unfortunately, we found that the NCX blocker ORM-10103 (77) exhibited a substantial block of I_f, precluding its inclusion in our preblocker mixture (*SI Appendix*, Fig. S7). However, it should be noted that, even if NCX is sensitive to ivabradine, the Ca^{2+}- and Na^+-channel blockers in our NCK mixture would have minimized NCX activity in our experiments. Overall, these observations underpin the difficulties in recording individual currents in native tissue and the need for more specific blockers of I_f.

Model Limitations.
Hodgkin–Huxley (HH) models for HCN1, HCN2, and I_f were used in this study so that we could take advantage of previously published models despite the limitations that HH models do not describe voltage-independent components of HCN-channel current (18, 19) and that they oversimplify of the kinetics of channel gating, which are more accurately fit with multistate gating models. Indeed, while the HH model of I_f we used provides reasonably good fits to steady-state voltage dependence, it would tend to overestimate the initial rates of activation and deactivation of I_f because it does not replicate the sigmoidal delays in gating that are characteristic of HCN channels (17). A limitation of our model

Peters et al.
Bidirectional flow of the funny current (I_f) during the pacemaking cycle in murine sinoatrial node myocytes

PNAS | 9 of 12
https://doi.org/10.1073/pnas.2104668118

www.manaraa.com

is that it shows a larger degree of gating of I_f (~20%) compared to experimental data in SAMs (negligible) or HEK cells (~5%). However, it is not clear that this discrepancy can be attributed to the initial rates of activation and deactivation. In the future, it will be informative to use multistate gating models to simulate changes in hyperpolarization-activated currents to investigate this issue and to probe the function of HCN channels in neurons, in which the voltage changes are much faster than in SAMs, and during changes in the AP firing pattern in SAMs, such as following sinus pauses or in response to autonomic stimulation.

Conclusions

Measurement of I_f during the sinoatrial AP is complicated by the large variability between AP waveforms in sinoatrial myocytes (21–23, 78). Thus, we measured I_f by applying APs recorded from the same cell as the voltage command as has been previously reported in DRG neurons (73) and ventricular myocytes (79). This approach has the advantage that the AP waveform is precisely matched to the ion channel expression in each cell. In contrast to the prevailing notion that I_f activates during the diastolic depolarization and deactivates during the subsequent AP, we show that I_f does not exhibit appreciable gating during the pacemaker cycle. These data highlight the AP-clamp technique as a powerful tool to record nonequilibrium properties of ion channels in native tissues and establish a new conceptual framework for pacemaking, in which I_f contributes substantial driving force in both directions.

Materials and Methods

Detailed methods are available in the *SI Appendix*.

Animal Ethics and Sinoatrial Node Dissociation. This study was carried out in accordance with the US Animal Welfare Act and the National Research Council's *Guide for the Care and Use of Laboratory Animals* (80) and was conducted according to a protocol that was approved by the University of Colorado Anschutz Medical Campus Institutional Animal Care and Use Committee. C57BL/6J mice were killed under anesthesia by cervical dislocation. SAMs were isolated by enzymatic and mechanical dissociation as previously described (24, 81, 82). Cells were stored at room temperature for up to 8 h before electrophysiological recordings.

Sinoatrial Myocyte Electrophysiology. Isolated SAMs were patch-clamped in the whole-cell configuration at 35 °C with continuous perfusion of extracellular solution. Spontaneous APs were recorded in current-clamp mode with zero injected current. Ca^{2+} currents were recorded in voltage-clamp mode using depolarizing voltage steps in a K^+ current–blocking extracellular solution as described previously (24). K^+ currents were measured in response to depolarizing steps in Tyrode's solution containing 3 μM isradipine to block voltage-gated Ca^{2+} currents. I_f recordings for use in modeling and studies of blocker effects were measured in recording Tyrode's solution containing either 1 nM or 1 μM isoproterenol as indicated. For AP-clamp recordings, SAMs were constantly perfused at 35 °C with recording Tyrode's extracellular solution containing 1 nM or 1 μM isoproterenol as indicated. Spontaneous APs were first recorded in the whole-cell current-clamp configuration, and then 10 s of the AP recording were included in the command-voltage protocol in voltage-clamp experiments to isolate the specific currents flowing during the AP (*SI Appendix*, Fig. S2). To account for an incomplete block of I_f by ivabradine, the subtracted currents during AP clamp were scaled for the measured fractional block achieved in the hyperpolarizing pulses from the same cell. In some cells, the current inhibited by ivabradine included a component of potassium current that remained in the blocker mixture as evidenced by an outward current evoked by a step to 0 mV from a holding potential of −40 mV (at which I_f is deactivated) or by

reversal potentials of the ivabradine-sensitive current that were substantially negative to the reversal potential for I_f under the same ionic conditions (Fig. 3D and *SI Appendix*, Fig. S3B). Analysis was restricted to cells in which no potassium current contamination was evident in the ivabradine-sensitive current.

HEK Cell Electrophysiology. HEK 293 cells stably expressing HCN4 (generously provided by Martin Biel's laboratory, Ludwig-Maximilians-Universität, Munich, Germany) were grown as previously described (83). Recordings were performed in the whole-cell configuration in recording Tyrode's extracellular solution with pipettes filled with a K-aspartate intracellular solution containing 0 or 1 mM cAMP as indicated. All recordings were performed at 35 °C.

Modeling. We modified an existing HH-type model of I_f in murine SAMs (47) and manually tuned the parameters to fit our experimental datasets obtained in SAMs in the presence of 1 nM or 1 μM isoproterenol. Detailed model equations are found in *SI Appendix, Supplementary Methods*, and the values of parameters used are reported in *SI Appendix*, Table S6. To model I_f during the sinoatrial AP, sets of 10 AP waveform recordings from the 1 nM and 1 μM isoproterenol AP-clamp experiments were used to stimulate the 1 nM and 1 μM isoproterenol models, respectively. Current–voltage relationships were calculated from the average of three consecutive APs. Model conductances were scaled such that the current amplitude at either −90 mV or −120 mV was the same as that experimentally recorded in the SAM from which the voltage protocol was derived. The model of HCN2 gating uses the equations from the non-cAMP–bound state of the model proposed by Wang et al. (51) The HCN1 model uses the gating scheme proposed by Battefeld et al. (50) Single-state HH-type models were chosen for HCN1 and HCN2 to be consistent with our models of I_f. The maximal conductances of the HCN1 and HCN2 models were scaled such that the maximal inward currents during AP-clamp simulations were similar to the 1 nM I_f model to facilitate comparisons of altered gating. All models were simulated in the Spyder Python environment using a forward Euler method with a 200-μs time step.

Analysis and Statistics. All analysis was performed in Clampfit 10.7 (Molecular Devices) with SigmaPlot 12.0 (SYSTAT Software) used for plotting. All statistical analysis was performed in JMP 14 (SAS Institute). The AP firing rate in response to ivabradine was evaluated with a repeated-measures ANOVA followed by a Tukey post hoc test with time following the application of ivabradine as the independent variable. The blockade of Ca^{2+} currents by ivabradine or isradipine was evaluated using paired t tests with the respective drug as the independent variable. Ivabradine and/or K^+-blocker mixture inhibition of transient and steady-state K^+ currents was evaluated with a repeated-measures ANOVA with the presence of specific blockers as the independent variable followed by a Tukey post hoc test for individual comparisons. To compare currents or charge movement of experimentally measured I_f and HCN4 in response to isoproterenol or cAMP, respectively, we used Student's t tests. Paired t tests were used to compare I_f or HCN4 current amplitude at −60 mV during the AP upstroke to the amplitude at −60 mV during AP repolarization in the same cells. Significance was determined at $P < 0.05$. All means, SEMs, and n values are provided in the text or in *SI Appendix*, Tables S1–S4.

Data Availability. All study data are included in the article and/or *SI Appendix*.

1. A. Keith, M. Flack, The form and nature of the muscular connections between the primary divisions of the vertebrate heart. *J. Anat. Physiol.* **41**, 172–189 (1907).
2. D. DiFrancesco, The contribution of the 'pacemaker' current (if) to generation of spontaneous activity in rabbit sino-atrial node myocytes. *J. Physiol.* **434**, 23–40 (1991).
3. H. F. Brown, D. DiFrancesco, S. J. Noble, How does adrenaline accelerate the heart? *Nature* **280**, 235–236 (1979).
4. T. M. Ishii, M. Takano, L. H. Xie, A. Noma, H. Ohmori, Molecular characterization of the hyperpolarization-activated cation channel in rabbit heart sinoatrial node. *J. Biol. Chem.* **274**, 12835–12839 (1999).
5. S. Moosmang, M. Biel, F. Hofmann, A. Ludwig, Differential distribution of four hyperpolarization-activated cation channels in mouse brain. *Biol. Chem.* **380**, 975–980 (1999).
6. S. Moosmang et al., Cellular expression and functional characterization of four hyperpolarization-activated pacemaker channels in cardiac and neuronal tissues. *Eur. J. Biochem.* **268**, 1646–1652 (2001).
7. I. Ragueneau et al., Pharmacokinetic-pharmacodynamic modeling of the effects of ivabradine, a direct sinus node inhibitor, on heart rate in healthy volunteers. *Clin. Pharmacol. Ther.* **64**, 192–203 (1998).

8. A. J. Camm, C.-P. Lau, Electrophysiological effects of a single intravenous administration of ivabradine (S 16257) in adult patients with normal baseline electrophysiology. *Drugs R D.* **4**, 83–89 (2003).

9. A. Bucchi, A. Barbuti, D. Difrancesco, M. Baruscotti, Funny current and cardiac rhythm: Insights from HCN knockout and transgenic mouse models. *Front. Physiol.* **3**, 240 (2012).

10. D. DiFrancesco, Funny channel gene mutations associated with arrhythmias. *J. Physiol.* **591**, 4117–4124 (2013).

11. A. O. Verkerk, R. Wilders, Pacemaker activity of the human sinoatrial node: an update on the effects of mutations in HCN4 on the hyperpolarization-activated current. *Int. J. Mol. Sci.* **16**, 3071–3094 (2015).

12. E. G. Lakatta, D. DiFrancesco, What keeps us ticking: a funny current, a calcium clock, or both? *J. Mol. Cell. Cardiol.* **47**, 157–170 (2009).

13. V. A. Maltsev, E. G. Lakatta, Synergism of coupled subsarcolemmal Ca2+ clocks and sarcolemmal voltage clocks confers robust and flexible pacemaker function in a novel pacemaker cell model. *Am. J. Physiol. Heart Circ. Physiol.* **296**, H594–H615 (2009).

14. D. DiFrancesco, The role of the funny current in pacemaker activity. *Circ. Res.* **106**, 434–446 (2010).

15. E. A. Accili, C. Proenza, M. Baruscotti, D. DiFrancesco, From funny current to HCN channels: 20 years of excitation. *News Physiol. Sci.* **17**, 32–37 (2002).

16. H. P. Larsson, How is the heart rate regulated in the sinoatrial node? Another piece to the puzzle. *J. Gen. Physiol.* **136**, 237–241 (2010).

17. C. Altomare *et al.*, Integrated allosteric model of voltage gating of HCN channels. *J. Gen. Physiol.* **117**, 519–532 (2001).

18. C. Proenza, D. Angoli, E. Agranovich, V. Macri, E. A. Accili, Pacemaker channels produce an instantaneous current. *J. Biol. Chem.* **277**, 5101–5109 (2002).

19. C. Proenza, G. Yellen, Distinct populations of HCN pacemaker channels produce voltage-dependent and voltage-independent currents. *J. Gen. Physiol.* **127**, 183–190 (2006).

20. A. O. Verkerk, R. Wilders, Hyperpolarization-activated current, If, in mathematical models of rabbit sinoatrial node pacemaker cells. *BioMed Res. Int.* **2013**, 872454 (2013).

21. D. DiFrancesco, A. Ferroni, M. Mazzanti, C. Tromba, Properties of the hyperpolarizing-activated current (if) in cells isolated from the rabbit sino-atrial node. *J. Physiol.* **377**, 61–88 (1986).

22. R. D. Nathan, Two electrophysiologically distinct types of cultured pacemaker cells from rabbit sinoatrial node. *Am. J. Physiol.* **250**, H325–H329 (1986).

23. M. R. Boyett, H. Honjo, I. Kodama, The sinoatrial node, a heterogeneous pacemaker structure. *Cardiovasc. Res.* **47**, 658–687 (2000).

24. E. D. Larson, J. R. St Clair, W. A. Sumner, R. A. Bannister, C. Proenza, Depressed pacemaker activity of sinoatrial node myocytes contributes to the age-dependent decline in maximum heart rate. *Proc. Natl. Acad. Sci. U.S.A.* **110**, 18011–18016 (2013).

25. C. H. Peters, E. J. Sharpe, C. Proenza, Cardiac pacemaker activity and aging. *Annu. Rev. Physiol.* **82**, 21–43 (2020).

26. N. Haechl, J. Ebner, K. Hilber, H. Todt, X. Koenig, Pharmacological profile of the bradycardic agent ivabradine on human cardiac ion channels. *Cell. Physiol. Biochem.* **53**, 36–48 (2019).

27. X. Wu *et al.*, Is ZD7288 a selective blocker of hyperpolarization-activated cyclic nucleotide-gated channel currents? *Channels (Austin)* **6**, 438–442 (2012).

28. C. F. Meier Jr, B. G. Katzung, Cesium blockade of delayed outward currents and electrically induced pacemaker activity in mammalian ventricular myocardium. *J. Gen. Physiol.* **77**, 531–547 (1981).

29. C. J. Abrams, N. W. Davies, P. A. Shelton, P. R. Stanfield, The role of a single aspartate residue in ionic selectivity and block of a murine inward rectifier K+ channel Kir2.1. *J. Physiol.* **493**, 643–649 (1996).

30. S. Zhang, S. J. Kehl, D. Fedida, Modulation of human ether-à-go-go-related K+ (HERG) channel inactivation by Cs+ and K+. *J. Physiol.* **548**, 691–702 (2003).

31. C. Valenzuela *et al.*, Class III antiarrhythmic effects of zatebradine. Time-, state-, use-, and voltage-dependent block of hKv1.5 channels. *Circulation* **94**, 562–570 (1996).

32. M. Baruscotti, A. Barbuti, A. Bucchi, The cardiac pacemaker current. *J. Mol. Cell. Cardiol.* **48**, 55–64 (2010).

33. J. L. Sánchez-Alonso, J. V. Halliwell, A. Colino, ZD 7288 inhibits T-type calcium current in rat hippocampal pyramidal cells. *Neurosci. Lett.* **439**, 275–280 (2008).

34. J. P. Lees-Miller *et al.*, Ivabradine prolongs phase 3 of cardiac repolarization and blocks the hERG1 (KCNH2) current over a concentration-range overlapping with that required to block HCN4. *J. Mol. Cell. Cardiol.* **85**, 71–78 (2015).

35. D. Melgari *et al.*, hERG potassium channel blockade by the HCN channel inhibitor bradycardic agent ivabradine. *J. Am. Heart Assoc.* **4**, e001813 (2015).

36. P. Bois, J. Bescond, B. Renaudon, J. Lenfant, Mode of action of bradycardic agent, S 16257, on ionic currents of rabbit sinoatrial node cells. *Br. J. Pharmacol.* **118**, 1051–1057 (1996).

37. C. Thollon *et al.*, Electrophysiological effects of S 16257, a novel sino-atrial node modulator, on rabbit and guinea-pig cardiac preparations: Comparison with UL-FS 49. *Br. J. Pharmacol.* **112**, 37–42 (1994).

38. A. Bucchi, M. Baruscotti, D. DiFrancesco, Current-dependent block of rabbit sino-atrial node I(f) channels by ivabradine. *J. Gen. Physiol.* **120**, 1–13 (2002).

39. J. Stieber, K. Wieland, G. Stöckl, A. Ludwig, F. Hofmann, Bradycardic and proarrhythmic properties of sinus node inhibitors. *Mol. Pharmacol.* **69**, 1328–1337 (2006).

40. A. Bucchi *et al.*, Identification of the molecular site of ivabradine binding to HCN4 channels. *PLoS One* **8**, e53132 (2013).

41. M. E. Mangoni *et al.*, Functional role of L-type Cav1.3 Ca2+ channels in cardiac pacemaker activity. *Proc. Natl. Acad. Sci. U.S.A.* **100**, 5543–5548 (2003).

42. M. Lei *et al.*, Requirement of neuronal- and cardiac-type sodium channels for murine sinoatrial node pacemaking. *J. Physiol.* **559**, 835–848 (2004).

43. M. V. Brahmajothi, M. J. Morales, D. L. Campbell, C. Steenbergen, H. C. Strauss, Expression and distribution of voltage-gated ion channels in ferret sinoatrial node. *Physiol. Genomics* **42A**, 131–140 (2010).

44. W. R. Giles, Y. Imaizumi, Comparison of potassium currents in rabbit atrial and ventricular cells. *J. Physiol.* **405**, 123–145 (1988).

45. D. DiFrancesco, A study of the ionic nature of the pace-maker current in calf Purkinje fibres. *J. Physiol.* **314**, 377–393 (1981).

46. D. DiFrancesco, Block and activation of the pace-maker channel in calf purkinje fibres: effects of potassium, caesium and rubidium. *J. Physiol.* **329**, 485–507 (1982).

47. S. Kharche, J. Yu, M. Lei, H. Zhang, A mathematical model of action potentials of mouse sinoatrial node cells with molecular bases. *Am. J. Physiol. Heart Circ. Physiol.* **301**, H945–H963 (2011).

48. D. DiFrancesco, Characterization of single pacemaker channels in cardiac sino-atrial node cells. *Nature* **324**, 470–473 (1986).

49. R. W. Tsien, Effects of epinephrine on the pacemaker potassium current of cardiac Purkinje fibers. *J. Gen. Physiol.* **64**, 293–319 (1974).

50. A. Battefeld, N. Rocha, K. Stadler, A. U. Bräuer, U. Strauss, Distinct perinatal features of the hyperpolarization-activated non-selective cation current I(h) in the rat cortical plate. *Neural Dev.* **7**, 21 (2012).

51. J. Wang, S. Chen, M. F. Nolan, S. A. Siegelbaum, Activity-dependent regulation of HCN pacemaker channels by cyclic AMP: signaling through dynamic allosteric coupling. *Neuron* **36**, 451–461 (2002).

52. T. M. Ishii, M. Takano, H. Ohmori, Determinants of activation kinetics in mammalian hyperpolarization-activated cation channels. *J. Physiol.* **537**, 93–100 (2001).

53. T. M. Ishii, N. Nakashima, K. Takatsuka, H. Ohmori, Peripheral N- and C-terminal domains determine deactivation kinetics of HCN channels. *Biochem. Biophys. Res. Commun.* **359**, 592–598 (2007).

54. J. Stieber *et al.*, Molecular basis for the different activation kinetics of the pacemaker channels HCN2 and HCN4. *J. Biol. Chem.* **278**, 33672–33680 (2003).

55. C. Altomare *et al.*, Heteromeric HCN1-HCN4 channels: a comparison with native pacemaker channels from the rabbit sinoatrial node. *J. Physiol.* **549**, 347–359 (2003).

56. A. Ludwig *et al.*, Two pacemaker channels from human heart with profoundly different activation kinetics. *EMBO J.* **18**, 2323–2329 (1999).

57. R. A. Capel, D. A. Terrar, The importance of Ca2+-dependent mechanisms for the initiation of the heartbeat. *Front. Physiol.* **6**, 80 (2015).

58. M. E. Mangoni, J. Nargeot, Genesis and regulation of the heart automaticity. *Physiol. Rev.* **88**, 919–982 (2008).

59. W. R. Giles, Supraventricular pacemaker activity in the canine heart: contributions from HCN channels in control conditions and in a model of heart failure. *Cardiovasc. Res.* **66**, 430–432 (2005).

60. A. O. Verkerk, A. C. G. van Ginneken, R. Wilders, Pacemaker activity of the human sinoatrial node: Role of the hyperpolarization-activated current, I(f). *Int. J. Cardiol.* **132**, 318–336 (2009).

61. M. Baruscotti *et al.*, A gain-of-function mutation in the cardiac pacemaker HCN4 channel increasing cAMP sensitivity is associated with familial Inappropriate Sinus Tachycardia. *Eur. Heart J.* **38**, 280–288 (2017).

62. Z. Liao, D. Lockhead, E. D. Larson, C. Proenza, Phosphorylation and modulation of hyperpolarization-activated HCN4 channels by protein kinase A in the mouse sinoatrial node. *J. Gen. Physiol.* **136**, 247–258 (2010).

63. J. R. St Clair, Z. Liao, E. D. Larson, C. Proenza, PKA-independent activation of I(f) by cAMP in mouse sinoatrial myocytes. *Channels (Austin)* **7**, 318–321 (2013).

64. M. Baruscotti *et al.*, Deep bradycardia and heart block caused by inducible cardiac-specific knockout of the pacemaker channel gene Hcn4. *Proc. Natl. Acad. Sci. U.S.A.* **108**, 1705–1710 (2011).

65. J. Alig *et al.*, Control of heart rate by cAMP sensitivity of HCN channels. *Proc. Natl. Acad. Sci. U.S.A.* **106**, 12189–12194 (2009).

66. S. Herrmann, J. Stieber, G. Stöckl, F. Hofmann, A. Ludwig, HCN4 provides a 'depolarization reserve' and is not required for heart rate acceleration in mice. *EMBO J.* **26**, 4423–4432 (2007).

67. E. Hoesl *et al.*, Tamoxifen-inducible gene deletion in the cardiac conduction system. *J. Mol. Cell. Cardiol.* **45**, 62–69 (2008).

68. S. Fenske *et al.*, cAMP-dependent regulation of HCN4 controls the tonic entrainment process in sinoatrial node pacemaker cells. *Nat. Commun.* **11**, 5555 (2020).

69. T.-L. Lu, T.-J. Lu, S.-N. Wu, Inhibitory perturbations of cilobradine (DK-AH269), A blocker of HCN channels, on the amplitude and gating of both hyperpolarization-activated cation and delayed-rectifier potassium currents. *Int. J. Mol. Sci.* **21**, 2416 (2020).

70. M. Manz, M. Reuter, G. Lauck, H. Omran, W. Jung, A single intravenous dose of ivabradine, a novel I(f) inhibitor, lowers heart rate but does not depress left ventricular function in patients with left ventricular dysfunction. *Cardiology* **100**, 149–155 (2003).

71. A. G. Torrente *et al.*, Burst pacemaker activity of the sinoatrial node in sodium-calcium exchanger knockout mice. *Proc. Natl. Acad. Sci. U.S.A.* **112**, 9769–9774 (2015).

72. L. Dini *et al.*, Selective blockade of HCN1/HCN2 channels as a potential pharmacological strategy against pain. *Front. Pharmacol.* **9**, 1252 (2018).

73. P. W. Liu, N. T. Blair, B. P. Bean, Action potential broadening in capsaicin-sensitive DRG neurons from frequency-dependent reduction of Kv3 current. *J. Neurosci.* **37**, 9705–9714 (2017).

74. T. Banyasz, B. Horvath, Z. Jian, L. T. Izu, Y. Chen-Izu, Sequential dissection of multiple ionic currents in single cardiac myocytes under action potential-clamp. *J. Mol. Cell. Cardiol.* **50**, 578–581 (2011).

Peters et al.
Bidirectional flow of the funny current (I$_f$) during the pacemaking cycle in murine sinoatrial node myocytes

www.manaraa.com

75. S. Groenke et al., Complete atrial-specific knockout of sodium-calcium exchange eliminates sinoatrial node pacemaker activity. *PLoS One* **8**, e81633 (2013).

76. Z. Gao et al., Genetic inhibition of Na+-Ca2+ exchanger current disables fight or flight sinoatrial node activity without affecting resting heart rate. *Circ. Res.* **112**, 309–317 (2013).

77. Z. Kohajda et al., The effect of a novel highly selective inhibitor of the sodium/calcium exchanger (NCX) on cardiac arrhythmias in in vitro and in vivo experiments. *PLoS One* **11**, e0166041 (2016).

78. C. Rickert, C. Proenza, Action potential heterogeneity in murine sinoatrial node myocytes. *Biophys. J.* **112**, 35a (2017).

79. Y. Chen-Izu, L. T. Izu, B. Hegyi, T. Bányász, "Recording of ionic currents under physiological conditions: Action potential-clamp and 'onion-peeling' techniques" in *Modern Tools of Biophysics, Handbook of Modern Biophysics*, T. Jue, Ed. (Springer, 2017), pp. 31–48.

80. National Research Council, *Guide for the Care and Use of Laboratory Animals* (National Academies Press, Washington, DC, ed. 8, 2011).

81. R. A. Rose, M. G. Kabir, P. H. Backx, Altered heart rate and sinoatrial node function in mice lacking the cAMP regulator phosphoinositide 3-kinase-γ. *Circ. Res.* **101**, 1274–1282 (2007).

82. E. J. Sharpe, J. R. St Clair, C. Proenza, Methods for the isolation, culture, and functional characterization of sinoatrial node myocytes from adult mice. *J. Vis. Exp.* **116**, 54555 (2016).

83. C. H. Peters et al., Isoform-specific regulation of HCN4 channels by a family of endoplasmic reticulum proteins. *Proc. Natl. Acad. Sci. U.S.A.* **117**, 18079–18090 (2020).

Peters et al.
Bidirectional flow of the funny current (I_f) during the pacemaking cycle in murine